Two-Factor Phase Separations in Mixed-Halide Quasi-2D Perovskite LEDs: Dimensionality and Halide Segregations

*Seok Joo Yang[1†], Kang Wang[1†], Yanqi Luo[2†], Jee Yung Park[1], Hanjun Yang[1], Aidan H. Coffey[3], Ke Ma[1], Jiaonan Sun[1], Sarah Wieghold[2], Chenhui Zhu[3], Letian Dou[1,4,5]**

[1]Davidson School of Chemical Engineering, Purdue University, West Lafayette, Indiana 47907, United States

[2]X-ray Science Division, Argonne National Laboratory, Lemont, Illinois 60439, United States

[3]Advanced Light Source, Lawrence Berkeley National Lab, Berkeley, California 94720, United States

[4]Department of Chemistry, Purdue University, West Lafayette, Indiana 47907, United States

[5]Birck Nanotechnology Center, Purdue University, West Lafayette, Indiana 47907, United States

[†]S. J. Yang, K. Wang and Y. Luo contributed equally.

*Corresponding Author: (L. Dou)

ABSTRACT

Quasi-2D halide perovskites have gained much interest as a promising material for light-emitting diodes (LEDs) due to their tunability in quantum confinement and halide alloy formation to modulate the energy bandgap and emission color. However, two-factor phase separations with respect to heterogeneous quantum-well thicknesses and halide segregation are still a crucial issue in quasi-2D perovskite LEDs, leading to low external quantum efficiencies (EQEs) and color shifts. Herein, we compare quasi-2D perovskite films using different cations to unveil the key contributions from the chemical design of organic cations. While mixing halide ions in conventional quasi-2D perovskite films induces micrometer scale heterogeneity, new extended and twisted conjugated cations suppress the two-factor phase separations, leading to high EQEs of over 25% and controllable emission wavelengths across red and near-infrared regions. The fundamental insights in this work will provide guidance for advancing materials design and device performance in the future.

TOC GRAPHICS

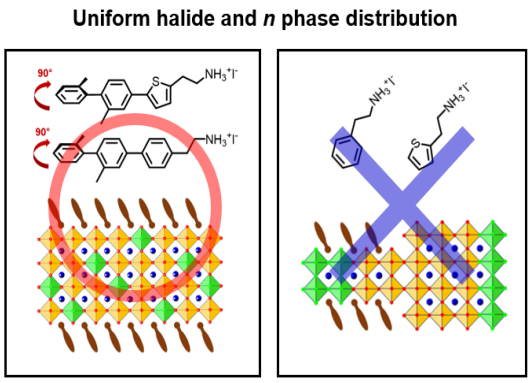

MAIN TEXT

Metal halide perovskite materials with ABX_3 crystal structure, where A indicates a small organic cation, B represents a metal cation and X is a halide anion, have been widely used in many applications due to their superior optoelectronic properties and remarkable tenability.[1-5] The energy bandgap of perovskite materials can be tuned and controlled by combining halide ions with various ratios, such as mixing I^- + Br^- or Br^- + Cl^-, allowing a wide coverage of photon absorption and emission throughout the visible light spectrum.[5-8] Mixed-halide perovskites have been intensively investigated in the fields of color-tunable light-emitting diodes (LEDs) and tandem solar cells.[5-7,9] However, mixed-halide perovskite thin films generally suffer from spatial heterogeneity of halide distributions, forming different kinds of halide-rich regions.[10-15] Halide segregation from ion migration contributes to nonuniform optoelectronic properties and low stability of the mixed-halide perovskite films. Therefore, inhibiting ion migration in mixed-halide perovskite films is critical to developing efficient and stable perovskite-based optoelectronic devices.[16,17]

To suppress ion migration in perovskite films, their lattice dimensionality can be tailored from 3D to layered 2D and further to 0D nanocrystals.[18-22] Among them, quasi-2D perovskite materials are emerging as a promising candidate owing to their unique quantum well structure and enhanced stabilities.[23-25] Quasi-2D perovskite materials adopt a general chemical formula of $L_2A_{n-1}B_nX_{3n+1}$, where L is a large organic cation, *n* is the number of inorganic BX_6^{4-} octahedra layers sandwiched between two large organic layers. The quantum well properties can be effectively modulated by controlling both the *n* number and composition of quasi-2D perovskites.[26] More importantly, incorporating large organic cations has been demonstrated to suppress ion diffusion in quasi-2D perovskite films.[27]

Recently, LEDs emitting at different wavelength regions have been achieved utilizing mixed-halide quasi-2D perovskite systems. However, managing two-factor phase separations which are a jumbled combination of halide species and *n*-phases in mixed-halide quasi-2D perovskite films remains a grand challenge because the nature of ionic bonds within the material enables ions to easily migrate in the crystal lattice and the formation of multiple-*n* phases in the film is thermodynamically favored.[28-30] Many research groups have been trying to overcome these two-factor phase separations issues by designing novel large organic ligands or manipulating the crystallization kinetics.[4,31-39] Nevertheless, the field still lacks a clear understanding on how

the organic ligands affect both distributions of *n*-phases and halide compositions, thus restricting further improvement in device performance.

In this work, we present a systematic approach to draw a clear physical picture of two distinct kinds of phase separations in mixed-halide quasi-2D perovskite films, thus yielding highly efficient wavelength-tunable LEDs with uniform phase distribution. Compared with conventional organic ligands, the newly synthesized organic ligands show well-suppressed two-factor phase separations. Molecular types and bulkiness of the organic ligands affect halide segregation and *n*-phase separation, which were imaged by nanoprobe X-ray fluorescence (n-XRF) and laser scanning confocal microscopy. We also uncover adverse effects of adding too much Br^- ions into the system which worsens *n*-phase separation, leading to declining device performances in mixed-halide quasi-2D perovskite LEDs. Therefore, systems with well-suppressed *n*-phase separation must be achieved before varying the Br^- composition to control the emission wavelengths of LED devices. These findings provide a deep understanding on how the organic ligands affect phase distributions, and could open up a new avenue for further improvement of mixed-halide quasi-2D perovskite based optoelectronic devices.

Mixing I^- and Br^- can induce inhomogeneity in 3D perovskite films resulting in local I-rich and Br-rich regions.[11] In addition, quasi-2D perovskite films may have nonuniform multi-*n* distributions.[28,32-37] Therefore, dual pathways of phase separations may occur in mixed-halide quasi-2D perovskites, and 4 plausible scenarios of film formation are illustrated in Scheme 1. "A type" shows uniform halide distribution with narrow *n* distribution, "B type" exhibits halide segregation with narrow *n* distribution, "C type" has uniform halide distribution but with *n* phase separation and "D type" depicts both halide and *n* phase separations. The primary goal is to achieve a mixed-halide quasi-2D perovskite film with uniformity closest to "A type" while understanding the role of organic ligands and thin film processing conditions to limit the two-factor phase separations in the films.

Two widely used organic ligands, thiophenylethylammonium iodide (TEA) and phenylethylammonium iodide (PEA), with their molecular structure shown in Figure 1a, were included in this work as references. To further examine how heteroatom (sulfur), conjugation length and molecular twist (planarity) affect the halide segregation and *n*-phase separation, we introduced 2-(5-(2,2′-dimethyl-[1,1′-biphenyl]-4-yl)thiophen-2-yl)ethyl-1-ammonium iodide (PPT),[40] and a newly synthesized 2-(2",3'-dimethyl-[1,1':4',1"-terphenyl]-4-yl)ethyl-1-ammounium iodide (PPP) with their chemical structures shown in Figure 1a. Different halide

compositions, nominal <*n*> numbers in precursor solution and processing conditions (e.g., annealing temperatures and interface materials) were systematically studied in this work.

We first examined the device performance incorporating different ligands and found that the new molecular design improved the device performance significantly. The complete LED device architecture is indium tin oxide (ITO) / Poly(N,N'-bis-4-butylphenyl-N,N'-bisphenyl)benzidine (Poly-TPD) / polyvinylpyrrolidone (PVP) / quasi-2D perovskite / 1,3,5-tris(1-phenyl-1H-benzimidazol-2-yl)benzene (TPBi) / LiF / Al (Figure 1b). For LED devices, the *n* number in quasi-2D perovskites highly affects device performances and emission wavelengths due to its quantum well structure.[28,32-37] In the aspect of external quantum efficiencies (EQE), nominal <*n*> = 4 is the optimum stoichiometric ratio for PPT and PPP based devices (Figure S1). In this system, the mixed-halide ratios of Br and I were controlled from pure Br to pure I. Photoluminescence (PL) spectra of thin films with Br-rich ratios show very low PL intensity compared to those with pure Br or I-rich ratios due to higher energy disorder in Br-rich films (Figure S2).[41] To achieve high EQEs of mixed-halide quasi-2D perovskite LEDs, the mixed-halide ratios were set as I-rich (I:Br) ratios of 10:0, 9:1, 6:1 and 3:1. Hereafter, the I:Br ratios are referred to as L100, L91, L61 and L31 (L: PPT, TEA, PPP and PEA), respectively, for convenience. To further increase EQE in mixed-halide quasi-2D perovskite LED, thermal annealing conditions, compositions, the thickness of hole and electron injection layers as well as passivation agents were fully optimized (Figures S3-7). Mixed-halide quasi-2D perovskite LEDs using PPT ligand all deliver EQEs of over 20% except for the 3:1 ratio (Figure 1c). Especially, PPT100 and PPT91 LED devices show high peak EQEs of 25.5% and 26.2%, respectively. Likewise, PPP LED devices also demonstrate high EQEs of nearly 20% except for the 3:1 ratio (Figure 1e). Thus, high ratio of Br^- ions (3:1) can decrease EQEs of mixed-halide quasi-2D perovskite LEDs using PPT and PPP ligands. On the other hand, no matter how much Br^- added, all TEA and PEA LED devices show lower EQEs of ~ 1% and 2% under similar processing conditions, respectively (Figure 1d and f). Current density-voltage-radiance curves and EQE statistics of all LED devices are shown in Figures S8 and S9.

Besides EQE results, the device emission profiles also exhibit distinct response to I/Br ratios. For example, electroluminescence (EL) spectra of PPT and PPP LED devices are gradually blue shifted as the amount of Br^- ions increases: 724, 716, 702 and 682 nm (PPT), and 730, 720, 706 and 679 nm (PPP) for 10:0, 9:1, 6:1 and 3:1 I:Br ratios, respectively (Figure 1g and i). In contrast, EL emission wavelengths of TEA and PEA based devices exhibit very small

shifts (Figure 1h and j) due to possible phase separation (formation of high *n* phase) and halide segregation (formation of I-rich domain). Correlation between the EL emission wavelength, EQE and the amount of Br^- ions shows that halide ratios must be carefully controlled in quasi-2D perovskite LEDs to achieve optimal performance. It is noteworthy that the device performace of PPT LEDs with I-rich compositions is competitive with other efficient quasi-2D perovskite LEDs (Figure S10). In addition, the operational stability of PPT and PPP LED devices is overall much higher than that of TEA and PEA LED devices (Figure S11). These devices serve as an excellent platform for further characterizing and elucidating the two-factor phase separation in mixed-halide quasi-2D perovskite systems.

To analyze the difference in the characteristics of quasi-2D perovskite LEDs, frequency-domain fluorescence lifetime imaging microscopy (FLIM) measurement was utilized to examine the optical homogeneity of the perovskite films. While PL intensity can be affected by the thickness of films, PL lifetime is considered as an intrinsic property of the materials, which gives precise images of phase distribution through lifetime mapping. FLIM measurement was carried out by fitting the lifetime of PL intensity to the selected area in a map with confocal PL microscope (Figure S12), thus lifetime maps can be compared with the PL images of the same areas. Mixed-halide quasi-2D perovskite films using PPT and PPP ligands show uniform PL intensity compared to TEA and PEA ligands (Figures 2 and S12). Although some dots with high and low PL intensities exist within small regions of PPT and PPP samples, they exhibit nearly identical lifetimes (Figures 2a and c, and S13). This suggests that this feature originates from topographic differences of polycrystalline films evident from atomic force microscopy (AFM) images rather than intrinsic differences in the material composition (Figure S14). On the other hand, homogeneity of PL intensity in TEA films is very poor regardless of the mixed-halide ratios, showing small particles of high PL intensity with background of low PL intensity (Figures 2b and f, and S13). Also, there are regions that have low PL intensities, but long lifetimes in TEA films. Since the 3D perovskites normally have longer PL lifetimes than 2D perovskites, the regions may originate from the 3D phase or a higher *n* phase compared to other regions. Likewise, there are some areas with longer PL lifetime in PEA samples shown as white colored regions in FLIM images for both 10:0 and 6:1 I:Br ratios (Figure 2d and h). On the contrary, red circled areas in Figure 2d show regions with high PL intensity and shorter PL lifetime from lower *n* phase compared to the rest. As the amount of Br^- ions increases, uniformity of PL intensity in PEA films decreases due to the formation of small particles (Figure S12). Small particles in TEA and PEA31 films are also

found in AFM images (Figure S14). However, whether the heterogeneity of PL intensity and morphology in TEA and PEA films comes from halide segregation or multi-*n* phase separation remains inconclusive only based on FLIM measurements. Since the lifetime depends on carrier density, power-dependent time-resolved PL between quasi-2D perovskite films was also compared in Figure S15.

Therefore, further characterizations were carried out to clarify origin of the inhomogeneity and the role of organic ligand design in regulating the two-factor phase separations. The evolution of halide heterogeneity in perovskite films was assessed using *in-situ* synchrotron-based n-XRF. The n-XRF measurement, using a 300 nm (full width at half maximum) focused X-ray beam at 14 keV, is sensitive in detecting trace concentrations of high-Z elements such as I, Br and Pb, but not the C, H and N in the perovskite films.[42] Owing to the long penetration length of high-energy X-ray photons, n-XRF can probe the elemental distribution in a buried layer in operational semiconducting devices, without exposing perovskite films directly to the incident X-ray beam as shown in Figure 3a.[43] The halide distributions in various perovskite LED devices under bias are shown in Figures 3b-e. To reduce beam-induced degradation during the *in-situ* measurement, an initial scan with a large pixel size was performed before applying bias which was followed by a fine scan with bias over the same region of the sample except for PPP61 film. As a result, degradation from the beam is negligible during repeating the measurement (Figure S16). Quasi-2D perovskite LED devices with I:Br = 6:1 ratio were selected for *in-situ* n-XRF characterization to satisfy the minimum amount of Br concentration required to exceed n-XRF detection limits without compromising performance as PPT61 and PPP61 LED devices possess high EQEs over 20%. While I distribution appears to be relatively uniform, Br distribution is heterogeneous in some of quasi-2D perovskite films (Figure S17). With 6:1 I:Br ratio, TEA shows a degree of bromine segregation before and after applying bias (Figure 3c), while the other organic ligands of PPT, PPP and PEA have homogenous Br distribution (Figure 3b, d and e). At a high voltage (8 V), EL spectra of TEA61 LED device is red-shifted (Figure S18), which may be from halide segregation by the bias, not *n* phase separation. TEA film starts halide-segregated even without the bias, as shown in the fine scan (Figure 3f). Both excess Br region (red circle) and Br-lacking region (blue circle) exist in the TEA film. The *in-situ* n-XRF data suggest that having the phenyl functional group within organic ligands can further aid in suppressing halide segregation, which is evident from homogenized halide distribution in PPT, PPP and PEA LED devices in contrast to halide-segregated TEA LED device.

To distinguish multi-*n* phase separation from halide segregation in these films, confocal PL images from different wavelength ranges were acquired to analyze the spatial distribution of different *n*-phases. Due to the difference in quantum confinement effects among different *n*-phases, small *n* numbers can be detected at shorter wavelength of PL spectra, while high *n* numbers and 3D phase can be seen at longer wavelength regions. PPT100 and PPP100 films do not show obvious 3D phase emissions and are dominated by high-*n* phase emission ranging from 597 nm to 695 nm (Figure 4a and c). On the other hand, the confocal images suggest that TEA100 and PEA100 films have significant amount of 3D phase mixed with small *n* phases formed as local particles, showing emissions from 553 nm to 597 nm (Figure 4b and d). Even in pure I systems, TEA and PEA ligands cannot effectively suppress the formation of multi-*n* phases compared to PPT and PPP ligands. As the amount of Br^- ions increases, the PL wavelengths of PPT and PPP films are shifted to shorter wavelength without 3D phase because *n* phase separation is well-suppressed (Figures S19-21). However, the ratio of 3D phase increases in TEA and PEA films proportional to the ratio of Br^- ions, even to an extent where 3D phase dominates over the ratio of small *n* numbers of quasi-2D perovskite in the films. Therefore, the *n* phase separation to 3D phase is accelerated by Br^- ions in TEA and PEA films, while PPT and PPP films maintain spatially homogeneous *n* distribution. To systematically gain insight on how molecular structure of ligands can affect *n* phase separation, PL and absorption spectra of quasi-2D perovskite films using two ligands of two-phenyl and two thiophene groups are also compared (Figure S22). Unfortunately, only extending the conjugation length cannot well-suppress ion migration in quasi-2D perovskite films since a more planar ligand with the same chemical formula as PPT also shows multi-*n* phases in the thin film due to difference in their effective bulkiness.[40] In conclusion, PPT and PPP ligands having extended and twisted molecular structures can efficiently suppress *n* phase separation compared to TEA and PEA ligands with short and simple moieties.

Overall PL spectra in PPT and PPP films show continuous shifts to shorter wavelength as the amount of Br^- ions increases (Figure S23a and b). In contrast, both small *n* numbers and 3D phase exist in TEA films with PL emissions from 520 nm to 600 nm for small *n* phases and from 700 nm to 850 nm for the 3D phase (Figure 5a). Both of the phases have shifted to shorter wavelength of PL spectra as adding more Br^- ions, which means Br^- ions are incorporated into both 2D and 3D phases. However, which dimension quantatively has more Br^- ions is difficult to be predicted by PL spectra.[44] Similarly, 3D phase exists in PEA films, although there is a negligible amount of small *n* phase observed in PEA100 film (Figure 5b). Likewise, as

indicated in X-ray diffraction (XRD) patterns, crystallinity of n = 2 phase in TEA films decreases in high Br ratio, while PEA films show 3D phase in PEA91 and PEA61 films (Figure 5c and d). Note that the crystallinity of quasi-2D perovskite films is low and some phases are missing in the XRD patterns. However, PEA films clearly show more 3D phase than TEA films. Thereby, PEA ligand is less effective in decreasing the 3D phase separation compared to TEA ligand in quasi-2D perovskite films. Because there is no strong peak in XRD pattern in PPT and PPP films (Figure S23c and d), grazing-incidence small-angle X-ray scattering (GISAXS) was performed to provide more structural information in PPT and PPP films (Figure S24). There is no major difference between the PPT and PPP films structurewise. Finally, even if PPT and PPP ligands can suppress the two-factor phase separations in most of the quasi-2D perovskite films with low Br^- concentration, there is still small n phase separation when more Br^- is added (e.g., the PPP31 film) as shown in the confocal PL mapping (Figure 5e). Empty spaces in short wavelength and brighter spaces in long wavelength at the same regions (red circles) means higher n number compared to other regions. In addition, there are smaller n phases (blue circles) in the film. The n phase separation can induce heterogeneity at 3:1 (I:Br) ratio, which may decrease EQE and operational stability of mixed-halide quasi-2D perovskite LED devices. These results indicate that the addition of Br^- ions in mixed-halide quasi-2D perovskite can induce further n phase separation, leading to red-shift in emission and decrease in EQE. In other words, this means that the two distinct processes are both highly intertwined by Br^- ions rather than clearly separated. Therefore, judicious materials and processing designs are needed to better control the two-factor phase separations. Note that energy transfer between uniform n distribution or 2D to 3D phases are compared by temperature-dependent PL spectra and transient absorption (TA) spectroscopy in Figure S25 and S26, respectively, and photoluminescence quantum yields of PPT and PPP films have higher than that of TEA and PEA films (Figure S27).

In summary, we have thoroughly investigated mixed-halide quasi-2D perovskite LEDs with 4 different ligands to understand and detangle the two-factor phase separations. Compared with the possible scenarios listed in the Scheme 1, most PPT and PPP films show “A type” of uniform halide distribution and narrow n distribution, while PPP31 film becomes more toward “C type”. TEA films show “D type” of the two-factor phase separations having both halide segregation and n phase separation. PEA films have high ratio of “C type” of n phase separation to 3D phase. Therefore, PPT and PPP ligands can better suppress the two-factor phase separations compared to TEA and PEA ligands in mixed-halide quasi-2D perovskite. Despite

the adverse effects observed from Br^- rich films, control over emission wavelength is acheived with adequate amounts of Br^- ions present with PPT and PPP ligands to suppress the two-factor phase separations. Accordingly, we were able to demonstrate highly efficient and color-tunable LED devices using PPT and PPP ligands. Depending on different ligands, possible mechanisms of phase separation in quasi-2D perovskites are suggested in Scheme S1. These results provide new insights in controlling the two-factor phase behaviors in mixed-halide quasi-2D perovskites and suggest new design criteria for future materials design and device optimization.

EXPERIMENTAL SECTION

Experimental details including materials, deposition of perovskite films, LED device fabrication, characterization and detailed measurement information are noted in the Supporting Information.

ASSOCIATED CONTENT

Supporting Information

The Supporting Information is available free of charge.

Experimental section including characterization and materials synthesis, and additional results with discussions in respect of J-V-R and EQE-J curves, EL and PL spectra, operational stability of LED devices, images of PL, PL lifetime and AFM, X-ray patterns, PLQY, characterizations of power-dependent TRPL, temperature-dependent PL and transient absorption, and the scheme for mechanism of phase separations

AUTHOR INFORMATION

Corresponding Author

Letian Dou – *Davidson School of Chemical Engineering, Department of Chemistry and Birck Nanotechnology Center, Purdue University, West Lafayette, Indiana 47907, United States*;

orcid.org/0000-0001-6411-8591; Email: dou10@purdue.edu

Authors

Seok Joo Yang – *Davidson School of Chemical Engineering, Purdue University, West Lafayette, Indiana 47907, United States*; orcid.org/0000-0002-0818-7813;

Kang Wang – *Davidson School of Chemical Engineering, Purdue University, West Lafayette, Indiana, 47907 United States*; orcid.org/0000-0002-7178-1225;

Yanqi Luo – *X-ray Science Division, Argonne National Laboratory, Lemont, Illinois 60439, United States*; orcid.org/0000-0001-5624-9583;

Jee Yung Park – *Davidson School of Chemical Engineering, Purdue University, West Lafayette, Indiana 47907, United States*; orcid.org/0000-0002-9814-6563;

Hanjun Yang – *Davidson School of Chemical Engineering, Purdue University, West Lafayette, Indiana 47907, United States*; orcid.org/0000-0002-6856-6559;

Aidan H. Coffey – *Advanced Light Source, Lawrence Berkeley National Lab, Berkeley, California 94720, United states*;

Ke Ma – *Davidson School of Chemical Engineering, Purdue University, West Lafayette, Indiana 47907, United States*; orcid.org/0000-0003-2168-0917;

Jiaonan Sun – *Davidson School of Chemical Engineering, Purdue University, West Lafayette, Indiana 47907, United States*; orcid.org/0000-0002-4102-0564;

Sarah Wieghold – *X-ray Science Division, Argonne National Laboratory, Lemont, Illinois 60439, United States*;

Chenhui Zhu – *Advanced Light Source, Lawrence Berkeley National Lab, Berkeley, California 94720, United states*; orcid.org/0000-0003-1263-5065;

Author Contributions

L.D. came up with the idea and supervised this project. S.J.Y. carried out device fabrications, PL analysis and data analysis and designed the project. K.W. synthesized PPT and TEA ligands and gave advice for the project. Y.L. and S.W. performed *in-situ* XRF measurement. J.Y.P.

carried out confocal PL and XRD measurements. H.Y. measured FLIM lifetime mapping, power-dependent time-resolved PL and TA spectroscopy. A. H. C. and C. Z. performed GISAXS characterizations. K.M. conducted AFM measurement. J.S. synthesized PPP ligand. S.J.Y. and L.D. wrote the manuscript, and all authors revised the manuscript.

ACKNOWLEDGMENTS

This work is supported by the National Science Foundation (Grant No. 2131608-ECCS and 2143568-DMR).

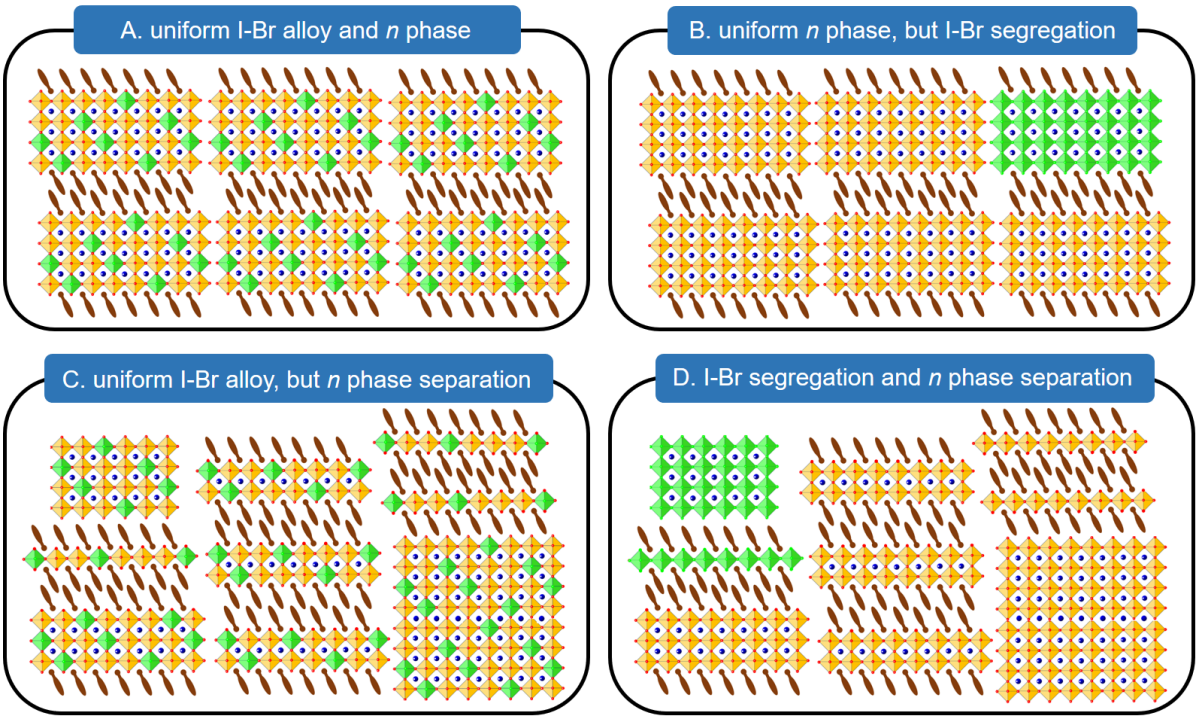

Scheme 1. Scheme of 4 possible phase distribution scenarios in mixed-halide quasi-2D perovskites. Yellow octahedral, $[PbI_6]^{4-}$; green octahedral, $[PbI_xBr_{6-x}]^{4-}$; brown line, organic ligand; and blue spheres, small organic cation.

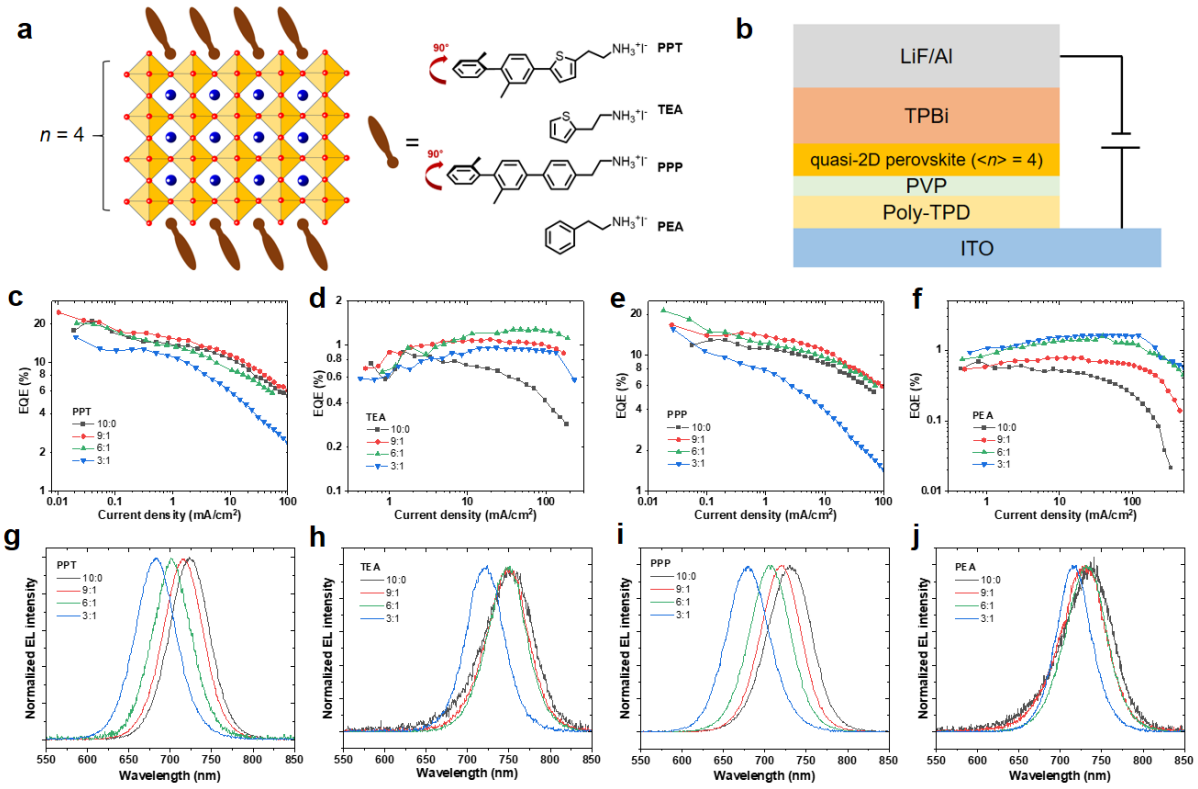

Figure 1. Ligand design and device characteristics. (a) Scheme of the quasi-2D perovskite layer (nominal <*n*> = 4) and 4 organic ligands of PPT, TEA, PPP and PEA. (b) Schematic diagram of LED device architecture. EQE characteristic of LED devices based on (c) PPT, (d) TEA, (e) PPP and (f) PEA ligands. Normalized EL spectra of (g) PPT, (h) TEA, (i) PPP and (j) PEA-based LED devices.

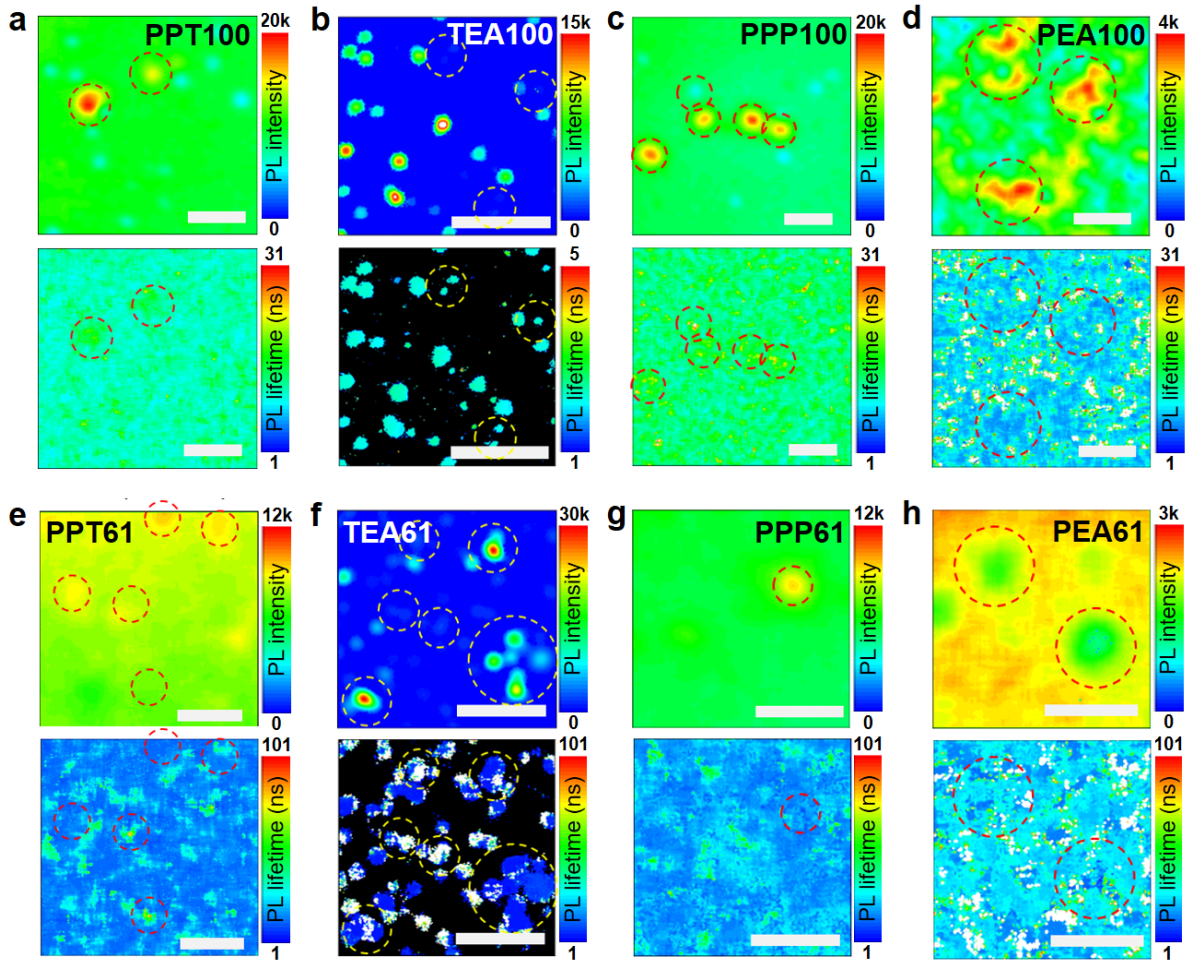

Figure 2. Homogeneity of the quasi-2D perovskite films in mixed-halide system. PL intensity (top) and PL lifetime (bottom) images of (a) PPT100, (b) TEA100, (c) PPP100 and (d) PEA100. PL intensity (top) and PL lifetime (bottom) images of (e) PPT61, (f) TEA61, (g) PPP61 and (h) PEA61 films. Scale bars: 20 μm.

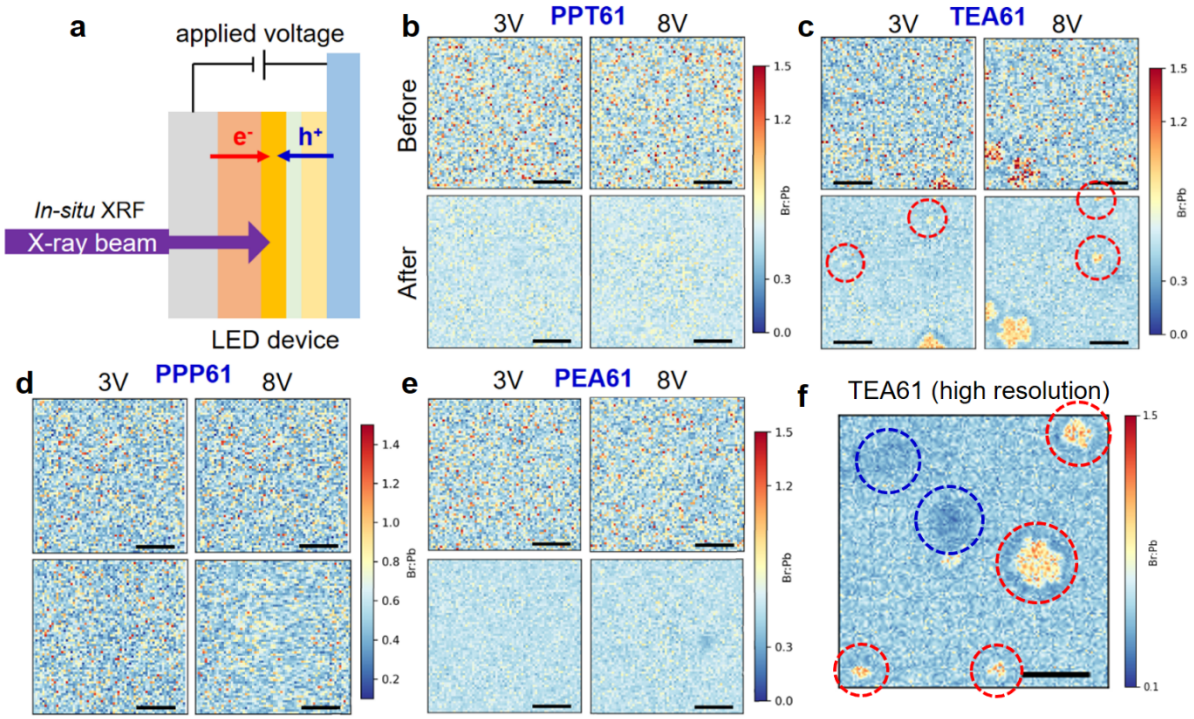

Figure 3. Resolving halide distribution under bias. (a) Scheme of *in-situ* XRF measurement. XRF mapping of (b) PPT61, (c) TEA61, (d) PPP61 and (e) PEA61 LED devices before and after applying voltage at 3 V and 8 V. (f) XRF mapping of TEA61 LED device at 0 V with high resolution. Scale bars: 5 μm.

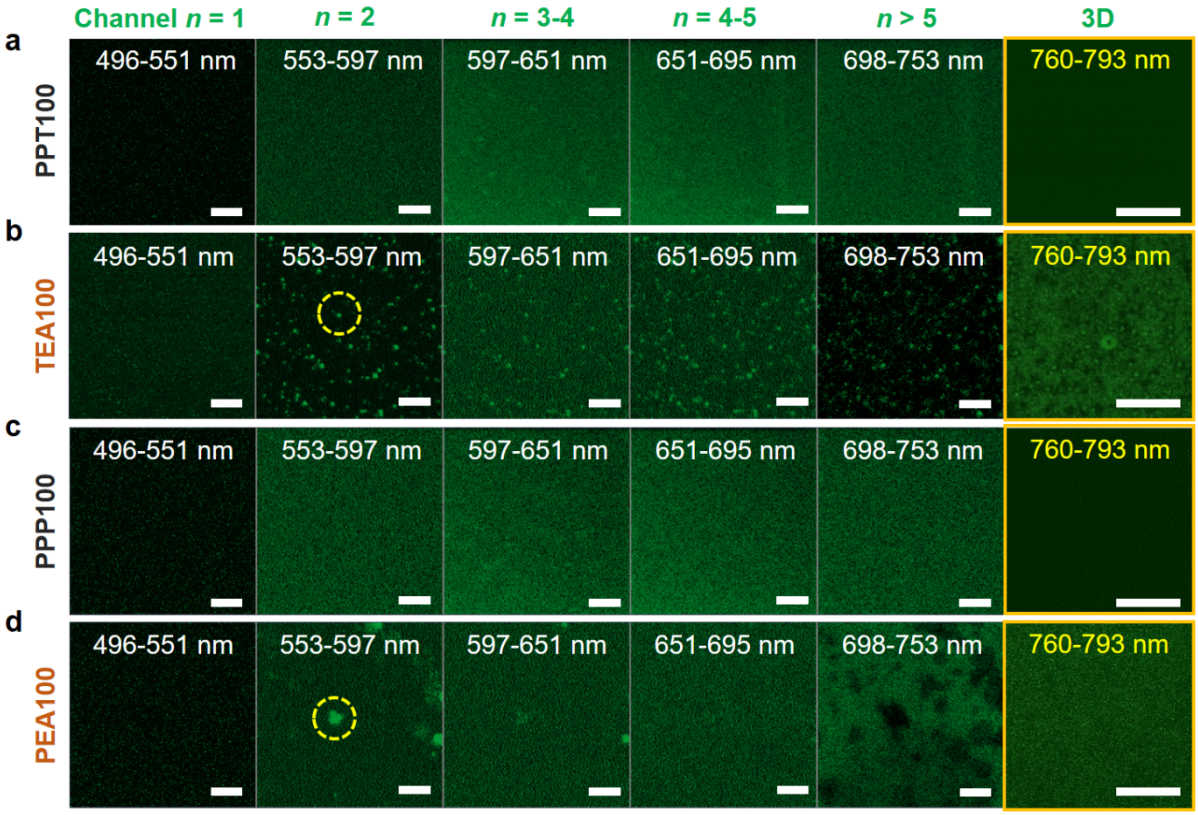

Figure 4. Visualizing *n* phase distribution in pure I system. Confocal PL images of (a) PPT100, (b) TEA100, (c) PPP100 and (d) PEA100 films. * Images in yellow frame were taken from different confocal PL measurement system in order to detect longer wavelength (760-793 nm). Scale bars: 20 μm.

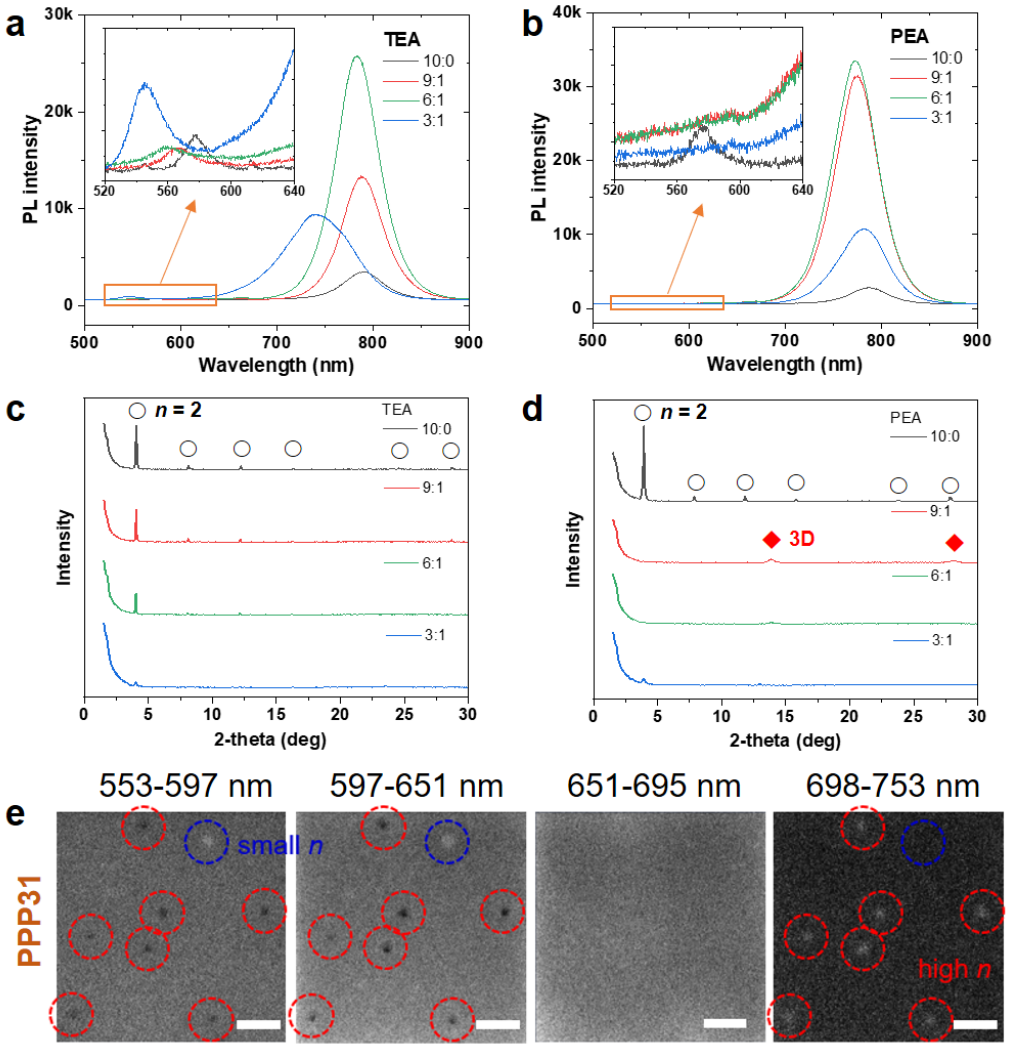

Figure 5. *n* phase distribution in mixed-halide systems. PL spectra of (a) TEA, (b) PEA films in mixed-halide system. XRD patterns of (c) TEA and (d) PEA films in mixed-halide system. (e) Confocal PL images of PPP31 film. Scale bars: 20 μm.

REFERENCES

(1) Hassan, Y.; Park, J.H.; Crawford, M.L.; Sadhanala, A.; Lee, J.; Sadighian, J.C.; Mosconi, E.; Shivanna, R.; Radicchi, E.; Jeong, M.; et al. Ligand-engineered bandgap stability in mixed-halide perovskite LEDs. *Nature* **2021**, *3*, 72-77.

(2) Tan, Z.-K.; Moghaddam, R.S.; Lai, M.L.; Docampo, P.; Higler, R.; Deschler, F.; Price, M.; Sadhanala, A.; Pazos, L.M.; Credgington, D.; et al. Bright light-emitting diodes based on organometal halide perovskite. *Nat. Nanotech*. **2014**, *9*, 687-692.

(3) Wang, C.; Han, D.; Wang, J.; Yang, Y.; Liu, X.; Huang, S.; Zhang, X.; Chang, S.; Wu, K.; Zhong, H. Dimension control of in situ fabricated $CsPbClBr_2$ nanocrystal films toward efficient blue light-emitting diodes. *Nat. Commun*. **2020**, *11*, 6428.

(4) Yang, S.J.; Kim, D.; Choi, J.; Kim, S.H.; Park, K.; Ryu, S.; Cho, K. Enhancing Thermoelectric Power Factor of 2D Organometal Halide Perovskites by Suppressing 2D/3D Phase Separation. *Adv. Mater.* **2021**, *33*, 2102797.

(5) Li, Z.; Chen, Z.; Yang, Y.; Xue, Q.; Yip, H.-L.; Cao, Y. Modulation of recombination zone position for quasi-two-dimensional blue perovskite light-emitting diodes with efficiency exceeding 5. *Nat. Commun.* **2019**, *10*, 1027.

(6) Vashishtha, P.; Halpert, J.E. Field-Driven Ion Migration and Color Instability in Red-Emitting 9Mixed Halide Perovskite Nanocrystal Light-Emitting Diodes. *Chem. Mater.* **2017**, *29* (14), 5965-5973.

(7) Vashishtha, P.; Ng, M.; Shivarudraiah, S.B.; Halpert, J.E. High Efficiency Blue and Green Light-Emitting Diodes Using Ruddlesden–Popper Inorganic Mixed Halide Perovskites with Butylammonium Interlayers. *Chem. Mater.* **2018**, *31* (1), 83-89.

(8) Liu, X.; Zhang, F.; Chang, S.; Wang, C.; Chen, C.; Sun, S.; Zhu, T.; Zhong, H. Bandgap and dimension regulation of $CsPbI_3$ perovskite through a bromine-terminated ligand for efficient pure red electroluminescence. *J. Mater. Chem. C* **2022**, *10*, 9707-9713.

(9) Gil-Escrig, L.; Dreessen, C.; Palazon, F.; Hawash, Z.; Moons, E.; Albrecht, S.; Sessolo, M.; Bolink, H.J. Efficient Wide-Bandgap Mixed-Cation and Mixed-Halide Perovskite Solar Cells by Vacuum Deposition. *ACS Energy Lett*. **2021**, *6* (2), 827-836.

(10) Barker, A.J.; Sadhanala, A.; Deschler, F.; Gandini, M.; Senanayak, S.P.; Pearce, P.M.; Mosconi, E.; Pearson, A.J.; Wu, Y.; Kandada, A.R.S.; et al. Defect-Assisted Photoinduced Halide Segregation in Mixed-Halide Perovskite Thin Films. *ACS Energy Lett.* **2017**, *2* (6), 1416-1424.

(11) Li, W.; Rothmann, M.U.; Liu, A.; Wang, Z.; Zhang, Y.; Pascoe, A.R.; Lu, J.; Jiang, L.; Chen, Y.; Huang, F.; et al. Phase Segregation Enhanced Ion Movement in Efficient Inorganic $CsPbIBr_2$ Solar Cells. *Adv. Energy Mater.* **2017**, *7*, 1700946.

(12) Slotcavage, D.J.; Karunadasa, H.I.; McGehee, M.D. Light-Induced Phase Segregation in Halide-Perovskite Absorbers. *ACS Energy Lett.* **2016**, *1* (6), 1199-1205.

(13) Hoke, E.T.; Slotcavage, D.J.; Dohner, E.R.; Bowring, A.R.; Karunadasa, H.I.; McGehee, M.D. Reversible photo-induced trap formation in mixed-halide hybrid perovskites for photovoltaics. *Chem. Sci.* **2015**, *6*, 613-617.

(14) Xiao, Z.; Kerner, R.A.; Zhao, L.; Tran, N.L.; Lee, K.M.; Koh, T.-W.; Scholes, G.D.; Rand, B.P. Efficient perovskite light-emitting diodes featuring nanometre-sized crystallites. *Nat. Photon.* **2017**, *11*, 108-115.

(15) Wang, Y.; Quintana, X.; Kim, J.; Guan, X.; Hu, L.; Lin, C.-H.; Jones, B.T.; Chen, W.; Wen, X.; Gao, H.; et al. Phase segregation in inorganic mixed-halide perovskites: from phenomena to mechanisms. *Photonics Res.* **2020**, *8* (11), A56-A71.

(16) Wang, Q.; Wang, X.; Yang, Z.; Zhou, N.; Deng, Y.; Zhao, J.; Xiao, X.; Rudd, P.; Moran, A.; Yan, Y.; et al. Efficient sky-blue perovskite light-emitting diodes via photoluminescence enhancement. *Nat. Commun.* **2019**, *10*, 5633.

(17) Shen, T.L.; Loganathan, A.; Do, T.H.; Wu, C.-M.; Chen, Y.-T.; Chen, Z.-J.; Chiu, N.-C.; Shih, C.-H.; Wang, H.-C.; Chou, J.-H.; et al. Characterize and Retard the Impact of the Bias-Induced Mobile Ions in $CH_3NH_3PbBr_3$ Perovskite Light-Emitting Diodes. *Adv. Opt. Mater.* **2021**, *10*, 2101439.

(18) Yuan, Z.; Hu, Z.; Persson, I.; Wang, C.; Liu, X.; Kuang, C.; Xu, W.; Bai, S.; Gao, F. Interface-assisted cation exchange enables high-performance perovskiteLEDs with tunable near-infrared emissions. *Joule* **2022**, *6* (10), 2423-2436.

(19) Kim, Y.-H.; Park, J.; Kim, S.; Kim, J.S.; Xu, H.; Jeong, S.-H.; Hu, B.; Lee, T.-W. Exploiting the full advantages of colloidal perovskite nanocrystals for large-area efficient light-emitting diodes. *Nat. Nanotechnol.* **2022**, *17*, 590-597.

(20) Kim, Y.-H.; Kim, S.; Kakekhani, A.; Park, J.; Park, J.; Lee, Y.-H.; Xu, H.; Nagane, S.; Wexler, R.B.; Kim, D.-H.; et al. Comprehensive defect suppression in perovskite nanocrystals for high-efficiency light-emitting diodes. *Nat. Photon.* **2021**, *15*, 148-155.

(21) Liang, A.; Wang, K.; Gao, Y.; Finkenauer, B.P.; Zhu, C.; Jin, L.; Huang, L.; Dou, L. Highly Efficient Halide Perovskite Light-Emitting Diodes via Molecular Passivation. *Angew. Chem. Int. Ed.* **2021**, *60*, 8337-8343.

(22) Yang, S.J.; Choi, J.; Song, S.; Park, C.; Cho, K. Enhancing air-stability and reproducibility of lead-free formamidinium-based tin perovskite solar cell by chlorine doping. *Sol. Energy Mater. Sol. Cells* **2021**, *227*, 111072.

(23) Quan, L.N.; Park, Y.; Guo, P.; Gao, M.; Jin, J.; Huang, J.; Copper, J.K.; Schwartzberg, A.; Schaller, R.; Limmer, D.T.; et al. Vibrational relaxation dynamics in layered perovskite quantum wells. *Proc. Natl. Acad. Sci.* **2021**, *118* (25), e2104425118.

(24) Quan, L.N.; Ma, D.; Zhao, Y.; Voznyy, O.; Yuan, H.; Bladt, E.; Pan, J.; Arquer, F.P.G.; Sabatini, R.; Piontkowski, Z.; et al. Edge stabilization in reduced-dimensional perovskites. *Nat. Commun.* **2020**, *11*, 170.

(25) Wang, K.; Jin, L.; Gao, Y.; Liang, A.; Finkenauer, B.P.; Zhao, W.; Wei, Z.; Zhu, C.; Guo, T.-F.; Huang, L.; et al. Lead-Free Organic-Perovskite Hybrid Quantum Wells for Highly Stable Light-Emitting Diodes. *ACS Nano* **2021**, *15* (4), 6316-6325.

(26) Wang, C.; Dai, G.; Wang, J.; Cui, M.; Yang, Y.; Yang, S.; Qin, C.; Chang, S.; Wu, K.; Liu, Y.; et al. Low-Threshold Blue Quasi-2D Perovskite Laser through Domain Distribution Control. *Nano Lett.* **2022**, *22* (3), 1338-1344.

(27) Shi, E.; Yuan, B.; Shiring, S.B.; Gao, Y.; Akriti; Guo, Y.; Su, C.; Lai, M.; Yang, P.; Kong, J.; et al. Two-dimensional halide perovskite lateral epitaxial heterostructures. *Nature* **2020**, *580*, 614-620.

(28) Xing, J.; Zhao, Y.; Askerka, M.; Quan, L.N.; Gong, X.; Zhao, W.; Zhao, J.; Tan, H.; Long, G.; Gao, L.; et al. Color-stable highly luminescent sky-blue perovskite light-emitting diodes. *Nat. Commun.* **2018**, *9*, 3541.

(29) Wang, N.; Cheng, L.; Ge, R.; Zhang, S.; Miao, Y.; Zou, W.; Yi, C.; Sun, Y.; Cao, Y.; Yang, R.; et al. Perovskite light-emitting diodes based on solution-processed self-organized multiple quantum wells. *Nat. Photon.* **2016**, *10*, 699-704.

(30) Shang, Y.; Li, G.; Liu, W.; Ning, Z. Quasi-2D Inorganic $CsPbBr_3$Perovskite for Efficient and Stable Light-Emitting Diodes. *Adv. Funct. Mater.* **2018**, *28*, 1801193.

(31) Ren, Z.; Yu, Z.; Qin, Z.; Wang, J.; Sun, J.; Chan, C.C.S.; Ding, S.; Wang, K.; Chen, R.; Wong, K.S.; et al. High-Performance Blue Perovskite Light-Emitting Diodes Enabled by Efficient Energy Transfer between Coupled Quasi-2D Perovskite Layers. *Adv. Mater.* **2021**, *33*, e2005570.

(32) Wang, Y.-K.; Ma, D.; Yuan, F.; Singh, K.; Pina, J.M.; Johnston, A.; Dong, Y.; Zhou, C.; Chen, B.; et al. Chelating-agent-assisted control of $CsPbBr_3$ quantum well growth enables stable blue perovskite emitters. *Nat. Commun.* **2020**, *11*, 3674.

(33) Chang, J.; Zhang, S.; Wang, N.; Sun, Y.; Wei, Y.; Li, R.; Yi, C.; Wang, J.; Huang, W. Enhanced Performance of Red Perovskite Light-Emitting Diodes through the Dimensional Tailoring of Perovskite Multiple Quantum Wells. *J. Phys. Chem. Lett.* **2018**, *9* (4), 881-886.

(34) Yuan, S.; Wang, Z.-K.; Xiao, L.-X.; Zhang, C.-F.; Yang, S.-Y.; Chen, B.-B.; Ge, H.-T.; Tian, Q.-S.; Jin, Y.; Liao, L.-S. Optimization of Low-Dimensional Components of Quasi-2D Perovskite Films for Deep-Blue Light-Emitting Diodes. *Adv. Mater.* **2019**, *31*, e1904319.

(35) Jin, Y.; Wang, Z.-K.; Yuan, S.; Wang, Q.; Qin, C.; Wang, K.-L.; Dong, C.; Li, M.; Liu, Y.; Liao, L.-S. Synergistic Effect of Dual Ligands on Stable Blue Quasi-2D Perovskite Light-Emitting Diodes. *Adv. Funct. Mater.* **2019**, *30*, 1908339.

(36) He, Z.; Liu, Y.; Yang, Z.; Li, J.; Cui, J.; Chen, D.; Fang, Z.; He, H.; Ye, Z.; Zhu, H.; et al. High-Efficiency Red Light-Emitting Diodes Based on Multiple Quantum Wells of Phenylbutylammonium-Cesium Lead Iodide Perovskites. *ACS Photonics* **2019**, *6* (3), 587-594.

(37) Gong, X.; Voznyy, O.; Jain, A.; Liu, W.; Sabatini, R.; Piontkowski, Z.; Walters, G.; Bappi, G.; Nokhrin, S.; Bushuyev, O.; et al. Electron-phonon interaction in efficient perovskite blue emitters. *Nat. Mater.* **2018**, *17*, 550-556.

(38) Yantara, N.; Jamaludin, N.F.; Febriansyah, B.; Giovanni, D.; Bruno, A.; Soci, C.; Sum, T.C.; Mhaisalkar, S.; Mathews, N. Designing the Perovskite Structural Landscape for Efficient Blue Emission. *ACS Energy Lett.* **2020**, *5* (5), 1593-1600.

(39) Xiao, Z.; Kerner, R.A.; Tran, N.; Zhao, L.; Scholes, G.D.; Rand, B.P. Engineering Perovskite Nanocrystal Surface Termination for Light-Emitting Diodes with External Quantum Efficiency Exceeding 15%. *Adv. Funct. Mater.* **2019**, *29*, 1807284.

(40) Wang, K.; Lin, Z.-Y.; Zhang, Z.; Jin, L.; Ma, K.; Coffey, A.H.; Atapattu, H.R.; Gao, Y.; Park, J.Y.; Wei, Z.; et al. Suppressing Phase Disproportionation in Quasi-2D Perovskite Light-Emitting Diodes. *Nat. Commun.* **2023**, *14*, 397.

(41) Seitz, M.; Meléndez, M.; York, P.; Kurtz, D.A.; Magdaleno, A.J.; Alcázar-Cano, N.; Kshirsagar, A.S.; Gangishetty, M.K.; Delgado-Buscalioni, R.; Congreve, D.N.; et al. Halide Mixing Inhibits Exciton Transport in Two-dimensional Perovskites Despite Phase Purity. *ACS Energy Lett.* **2022**, *7* (1), 358-365.

(42) Correa-Baena, J.-P.; Luo, Y.; Brenner, T.M.; Snaider, J.; Sun, S.; Li, X.; Jensen, M.A.; Hartono, N.T.P.; Nienhaus, L.; Wieghold, S.; et al. Homogenized halides and alkali

cation segregation in alloyed organic-inorganic perovskites, *Science* **2019**, *363* (6427), 627-631.

(43) Kodur, M.; Kumar, R.E.; Luo, Y.; Cakan, D.N.; Li, X.; Stuckelberger, M.; Fenning, D.P. X-Ray Microscopy of Halide Perovskites: Techniques, Applications, and Prospects, *Adv. Energy Mater*. **2020**, *10*, 1903170.

(44) Wright, N.E.; Qin, X.; Xu, J.; Kelly, L.L.; Harvey, S.P.; Toney, M.F.; Blum, V.; Stiff-Roberts, A.D.; Influence of Annealing and Composition on the Crystal Structure of Mixed-Halide, Ruddlesden-Popper Perovskites, *Chem. Mater*. **2022**, *34*, 3109-3122.